Threshold collision-induced dissociation of $Sr^{2+}(H_2O)_x$ complexes ($x=1-6$): An experimental and theoretical investigation of the complete inner shell hydration energies of Sr^{2+}

D. R. Carl, B. K. Chatterjee,[a] and P. B. Armentrout[b]
Department of Chemistry, University of Utah, 315 S. 1400 E. Room 2020, Salt Lake City, Utah 84112, USA

(Received 22 September 2009; accepted 22 December 2009; published online 26 January 2010)

The sequential bond energies of $Sr^{2+}(H_2O)_x$ complexes, where $x=1-6$, are determined by threshold collision-induced dissociation using a guided ion beam tandem mass spectrometer equipped with an electrospray ionization source. The electrospray source produces an initial distribution of $Sr^{2+}(H_2O)_x$ complexes, where $x=6-9$. Smaller $Sr^{2+}(H_2O)_x$ complexes, where $x=1-5$, are accessed using a recently developed in-source fragmentation technique that takes place in the high pressure region of a rf-only hexapole ion guide. This work constitutes the first experimental study for the complete inner shell of any multiply charged ion. The kinetic energy dependent cross sections are determined over a wide energy range to monitor all possible dissociation products and are modeled to obtain 0 and 298 K binding energies for loss of a single water molecule. These binding energies decrease monotonically for the $Sr^{2+}(H_2O)$ complex to $Sr^{2+}(H_2O)_6$. Our experimental results agree well with previous literature results obtained by equilibrium and kinetic studies for $x=5$ and 6. Because there has been limited theory for the hydration of Sr^{2+}, we also present an in-depth theoretical study on the energetics of the $Sr^{2+}(H_2O)_x$ systems by employing several levels of theory with multiple effective core potentials for Sr and different basis sets for the water molecules.
© *2010 American Institute of Physics*. [doi:10.1063/1.3292646]

I. INTRODUCTION

Water is an essential component in all forms of life. Bulk water forms an intricate hydrogen bonding network that becomes disrupted in the presence of metal cations as the electronegative oxygen atoms are directed toward the positively charged metal center. The ionic radius of the metal cation determines the number of water molecules that coordinate directly to the metal cation in the inner hydration shell as well as the binding affinities of those water molecules. Once the inner shell is filled, additional water molecules interact with these inner shell water molecules through hydrogen bonds. Investigating metal ion hydration in the gas phase provides a suitable environment to acquire fundamental thermodynamic information of these important metal ion-water interactions, which cannot be determined in the liquid phase.

Gas-phase studies of hydrated alkaline earth metal dications have become attractive systems for experimentalists as these ions can be generated readily with electrospray ionization (ESI).[1–7] The hydration energies for $Sr^{2+}(H_2O)_x$, where $x=5-14$, have been determined previously by equilibrium experiments using high pressure mass spectrometry[3] (HPMS) and kinetic studies using blackbody infrared dissociation (BIRD).[5] The thermodynamics for the more tightly bound water molecules ($x=1-4$) have not been determined as these smaller complexes pose a significant experimental challenge to such temperature-dependent techniques. Alternatively, guided ion beam mass spectrometry[8] lends itself to this problem because the reactivity of ion-molecule complexes is investigated as a function of kinetic energy, which can be varied over a much broader range than temperature.

The present work comprises a complete experimental investigation of the hydration energies of $Sr^{2+}(H_2O)_x$, where $x=1-6$, using threshold collision-induced dissociation (TCID). $Sr^{2+}(H_2O)_x$ ions are formed readily using ESI, but can also be generated in a dc discharge flow tube ion source (DC/FT).[9] Because strontium's second ionization energy (11.0 eV) lies below the first ionization energy of water (12.6 eV),[10] association of Sr^{2+} with H_2O in the flow tube can form $Sr^{2+}(H_2O)_x$ complexes whereas charge transfer would otherwise dominate the interaction. Qualitative comparisons are made between TCID results from $Sr^{2+}(H_2O)_x$ complexes generated with both the ESI and DC/FT sources, which demonstrates that the ESI source provides more reliable quantitative results.

Compared to the number of theoretical studies of $Mg^{2+}(H_2O)_x$ and $Ca^{2+}(H_2O)_x$ complexes, relatively little has been done for the $Sr^{2+}(H_2O)_x$ complexes. Glendening and Feller[11] have performed geometry optimizations and single point energies on $Sr^{2+}(H_2O)_x$ complexes, where $x=1-6$. Independent studies by Klobukowski,[12] Bauschlicher and co-workers,[13] and Kaupp and Schleyer[14] have determined binding energies for Sr^{2+} bound to $x=1-4$, $x=1-3$, and $x=1-2$ water molecules, respectively, using a variety of basis set treatments. The present work includes a rigorous theoretical assessment of the binding enthalpies of all $Sr^{2+}(H_2O)_x$ complexes studied here utilizing two different effective core potentials (ECPs) on Sr. By employing multiple levels of theory with different basis set treatments for the $Sr^{2+}(H_2O)_x$

[a]Present address: Bose Institute. West Bengal. India.
[b]Electronic mail: armentrout@chem.utah.edu.

 © 2010 American Institute of Physics

Downloaded 02 Dec 2010 to 155.97.11.184. Redistribution subject to AIP license or copyright; see http://jcp.aip.org/about/rights_and_permissions

system, we are able to determine specific combinations that are capable of reproducing our experimental hydration energies for these tightly bound water molecules. Such agreement provides additional support for the successful application of TCID studies for such multiply charged systems as well as confirmation that the ESI source produces thermalized ions.

II. EXPERIMENTAL AND COMPUTATIONAL SECTION

A. General experimental procedures

Cross sections for the CID of $Sr^{2+}(H_2O)_x$ complexes are measured using a guided ion beam tandem mass spectrometer (GIBMS), which has been described in detail previously.[8,15] Hydrated complexes are produced using an ESI source[16,17] by syringe pumping a $10^{-4}M$ solution of $SrCl_2$ dissolved in high performance liquid chromatography (HPLC) water through a 35 gauge stainless steel electrospray emitter set to ~2000 V with respect to an inlet cap, which serves as the counterelectrode. Ions are first passed through a heated capillary set at 80 °C and subsequently injected into an ion funnel.[18] The ion funnel transmits ions through the high pressure region of the source via a gentle dc voltage gradient and radially focuses the ions into a tight beam via opposite phases of radio frequency (rf) voltage on adjacent ion funnel plates. Ions are then injected into a rf-only hexapole where the ions undergo multiple collisions ($>10^4$) with the ambient gas and become thermalized. The internal energies of reactant ions produced by the ESI source can be described by a Maxwell–Boltzmann distribution at 300 K, as characterized by previous experiments and the results below.[7,17,19–21]

The ESI source produces an initial distribution of $Sr^{2+}(H_2O)_x$ complexes in which $x=6-9$ are formed with reasonable intensity. Smaller $Sr^{2+}(H_2O)_x$ complexes, where $x=1-5$, are produced via an in-source fragmentation technique that takes place in the high pressure region of the hexapole ion guide, as described previously for the $Ca^{2+}(H_2O)_x$ system.[22] Briefly, this technique utilizes negative voltages on a set of 0.25 in. dc electrodes placed between the hexapole rods to induce fragmentation of the initial distribution. The electrode assembly produces smaller $Sr^{2+}(H_2O)_x$ complexes under conditions that have been shown to form thermalized complexes at 300 K.[22] This conclusion is also tested below.

$Sr^{2+}(H_2O)_x$, where $x=1-6$, could also be generated using a DC/FT.[9] In the DC/FT source, strontium dications are generated at the cathode, a tantalum boat filled with the strontium metal located at the head of a 1 m long flow tube, by using a continuous dc discharge with typical operating conditions of 1.9–2.2 kV and 10–20 mA. The metal dications are carried down the flow tube by a buffer gas (ca. 10% argon in helium) with normal operating pressures of 0.3–0.4 Torr. About 50 cm downstream from the discharge, water vapor is introduced into the flow tube and the complexes of interest are formed via three-body associative reactions in the flow of the He/Ar carrier gas. For singly charged species, complex ions formed in the DC/FT source are thermalized to 300 K (the temperature of the flow tube) by undergoing $\sim 10^5$ collisions with the buffer gases as they drift along the 1 m long flow tube.[23–30]

$Sr^{2+}(H_2O)_x$ ions are extracted from the source and mass selected using a magnetic momentum analyzer. Ions are then decelerated to well-defined kinetic energies and focused into a rf octopole ion guide, trapping the ions radially.[8,31,32] The octopole minimizes reactant and product ion loss resulting from scattering. The octopole passes through a collision cell containing the collision gas, xenon, which is used for reasons outlined elsewhere.[33,34] Product ions formed in these collisions and unreacted parent ions drift to the end of the octopole where they are focused, mass selected using a quadrupole mass filter, and detected by a scintillation ion detector capable of single ion counting.[35]

Ion intensities are converted to absolute cross sections as described previously.[8] The uncertainty in the absolute cross sections is estimated at ±20%. In the octopole region, ions are accelerated by V_{Lab}, the voltage difference between the dc bias on the octopole ion guide and the ion source. Because the ions are doubly charged, their kinetic energy in the laboratory frame is twice this voltage, $E_{Lab}=2\times V_{Lab}$. Energies in the laboratory frame (Lab) are converted to center-of-mass (CM) collision energies by $E_{CM}=E_{Lab}\times m/(m+M)$, where m and M represent the mass of the neutral collision gas and ionic reactant, respectively. The absolute zero of energy for the ion beam is determined using a retarding potential technique.[8] The derivative of the transmission curve, which describes the kinetic energy distribution of the reactant ion beam, is then fit to a Gaussian distribution with a full width at half-maximum (FWHM) ranging from 0.10 to 0.15 eV. The uncertainty in the absolute energy scale is 0.05 eV (Laboratory). All energies in this paper are in the CM frame unless specified otherwise.

B. Thermochemical analysis

The kinetic energy dependent cross sections for single water molecule loss from a parent $Sr^{2+}(H_2O)_x$ complex are modeled using the empirical threshold model shown in Eq. (1):

$$\sigma(E) = \sigma_0 \sum g_i(E + E_i - E_0)^n/E, \quad (1)$$

where σ_0 is an energy independent scaling factor, E is the relative translational energy of the ion, E_0 is the reaction threshold at 0 K, and n is an adjustable fitting parameter that describes the efficiency of the energy transfer upon collision.[15] The summation is over the rovibrational states of the reactants having excitation energies, E_i, and populations, g_i, where $\Sigma g_i=1$. Vibrational frequencies and rotational constants are taken from the *ab initio* calculations discussed below. The Beyer–Swinehart–Stein–Rabinovich algorithm is used to evaluate the internal energy distribution for the reactants.[36–39] The relative populations, g_i, are computed for a Maxwell–Boltzmann distribution at 300 K.

To produce accurate thermochemical data from the modeling of the CID process, we must consider a number of effects such as those arising from multiple collisions, lifetime effects, and energy distributions. To ensure rigorous

Downloaded 02 Dec 2010 to 155.97.11.184. Redistribution subject to AIP license or copyright; see http://jcp.aip.org/about/rights_and_permissions

single collision conditions, cross sections are obtained at multiple pressures of Xe, typically 0.20, 0.10, and 0.05 mTorr in these studies, and extrapolated to zero pressure cross sections.[23,40] As the $Sr^{2+}(H_2O)_x$ ions become larger, ions with energy in excess of the threshold energy may not have time to dissociate on the time scale of the experiment, τ, about 5×10^{-4} s.[15] This leads to a kinetic shift in the energy threshold obtained from our modeling. To account for this effect, we incorporate Rice–Ramsperger–Kassel–Marcus (RRKM) statistical theory[39,41,42] for unimolecular dissociation into Eq. (1), as discussed in detail previously[43–45] and shown in Eq. (2),

$$\sigma(E) = \left(\frac{n\sigma_o}{E}\right)\sum_i g_i \int_{E_o-E_i}^{E} [1-e^{-k(\varepsilon+E_i)\tau}](E-\varepsilon)^{n-1} d\varepsilon. \tag{2}$$

Here, ε represents the energy deposited into the ion upon collision with xenon and $k(\varepsilon+E_i)=k(E^*)$ is the RRKM unimolecular dissociation rate constant shown in Eq. (3),

$$k(E^*) = sN_{vr}^{\dagger}(E^*-E_0)/h\rho_{vr}(E^*). \tag{3}$$

Here s is the reaction degeneracy calculated from the ratio of rotational symmetry numbers of the reactants with respect to the products, $N_{vr}^{\dagger}(E^*-E_0)$ is the sum of the rovibrational states of the transition state (TS) at an energy E^*-E_0 above the threshold, and $\rho_{vr}(E^*)$ is the density of rovibrational states for the energized molecule (EM) at the energy available, E^*. When the rate constant is much faster than the average experimental time scale, Eq. (2) reduces to Eq. (1). The integration in Eq. (2) is over the excitation energy distribution, which is a function of the impact parameter between the ion and xenon gas. Equation (2) has been shown to accurately describe kinetic shifts in a number of previous CID experiments.[19–21,29,30,46–49]

The calculation of the RRKM unimolecular rate constant requires the rovibrational states of the EM and TS.[39,41,42] The molecular parameters for the EM are taken from *ab initio* calculations of the reactant ion. The TS is assumed to be loose with no reverse activation barrier, as is appropriate for the heterolytic bond cleavages studied here.[50] Thus, the phase-space limit (PSL) TS is productlike using molecular parameters taken from *ab initio* calculations of the products. For the $Sr^{2+}(H_2O)_x$ complexes, the transitional modes, those that become rotations of the dissociated products, are treated as rotors and calculated from the rotational constants of the separate dissociation products, $Sr^{2+}(H_2O)_{x-1}$ and H_2O. The external rotational constants and rotational energy of the TS are determined by assuming that the TS is located at the centrifugal barrier for the interaction of $Sr^{2+}(H_2O)_{x-1}$ and H_2O, and calculated using a variational approach as outlined elsewhere.[45] The data analysis program used (CRUNCH) accurately accounts for the charge on the ion in determining the location of the centrifugal barrier. The two-dimensional (2D) external rotations are treated adiabatically, but include centrifugal effects.[51] Here, the adiabatic 2D external rotational energy of the EM is calculated using a statistical distribution with an explicit summation over the possible values of the rotational quantum number.[45]

The model CID cross sections of Eqs. (1) and (2) are convoluted over the kinetic energy distributions of the $Sr^{2+}(H_2O)_x$ complex and xenon gas, then compared with the experimental cross sections.[8] A nonlinear least-squares fitting procedure is used to optimize the fitting parameters, σ_0, n, and E_0. Because E_0 represents the minimum amount of energy required to go from reactants to products at 0 K, this reaction threshold represents the binding energy of the water molecule to the complex. This assumes that there are no activation barriers beyond the endothermicity of the reaction, which is ordinarily the case for heterolytic bond cleavages such as those studied here.[50] The uncertainties in the modeling parameters are determined from additional modeling of the cross sections by scaling the *ab initio* vibrational frequencies up and down by 10%, varying the best fit n value up and down by 0.1, and if lifetime effects are taken into account, by scaling the average experimental time available for dissociation up and down by a factor of 2. The absolute uncertainty of the energy scale (0.05 eV laboratory) is also included in the uncertainties for E_0.

C. Computational details

Calculations were performed with GAUSSIAN03 (Ref. 52) unless specified otherwise. Geometries determined previously for $Ca^{2+}(H_2O)_x$ complexes[7] served as starting structures for the $Sr^{2+}(H_2O)_x$ complexes. For the $Sr^{2+}(H_2O)_x$ complexes, geometry optimizations were performed at the B3LYP[53,54] level of theory with the HW*/6-311+G(d,p) basis set. Here, the HW* indicates that Sr was described using an ECP and valence basis set from Hay and Wadt[55] with a single d polarization function (exponent of 0.40) added.[11] Water molecules were treated with the 6-311+G(d,p) basis set. For comparison, geometry optimizations were also performed with three additional levels of theory: B3LYP/SD/6-311+G(d,p), B3LYP/Def2TZVP, and BH&HLYP/Def2TZVPP. The former uses the Stuttgart-Dresden (SD)ECP and basis set for Sr developed by Kaupp *et al.*[56] and the 6-311+G(d,p) basis set for water, whereas in the latter, all atoms are represented by the Def2TZVP basis set,[57] a balanced set of triple zeta+polarization functions quality that also uses the SD ECP for Sr, or the Def2TZVPP basis set that includes extra valence functions for Sr and H atoms, but none for O atoms. Both ECPs in this work utilize a small core of 28 electrons. Vibrational frequencies and rotational constants were also calculated with these basis set treatments. Frequencies were scaled by 0.989 to calculate zero-point energy and thermal corrections.[58] Single point energies were subsequently calculated at the B3LYP, B3P86,[59] MP2(full),[60] and M06 (Ref. 61) levels using the HW*/6-311+G(2d,2p) (HW*), SD/6-311+G(2d,2p) (SD), and Def2TZVPP basis sets. M06 single point energies were calculated using NWChem.[62] Basis set superposition errors (BSSE) corrections in the bond dissociation energies were calculated using the full counterpoise (cp) method.[63,64]

Relaxed potential energy surface and synchronous transit-guided quasi-Newton[65] calculations were also per-

Downloaded 02 Dec 2010 to 155.97.11.184. Redistribution subject to AIP license or copyright; see http://jcp.aip.org/about/rights_and_permissions

formed to map out the reaction coordinates of the charge separation process from $Sr^{2+}(H_2O)_2$. TSs and intermediate structures were optimized at the B3LYP/HW*/6-311+G(d,p), B3LYP/SD/6-311+G(d,p), and B3LYP/Def2TZVP levels of theory. Single point energies of TS and intermediate structures were calculated at the B3LYP and MP2(full) levels with the HW*/6-311+G(2d,2p), SD/6-311+G(2d,2p), and Def2TZVPP basis sets. All energies include zero point energy (ZPE) corrections.

III. RESULTS

A. Cross sections for collision-induced dissociation

The CID cross sections for $Sr^{2+}(H_2O)_x$, where $x=1-6$, are shown in Fig. 1. In all cases, the dominant reaction is the loss of a single water molecule, as shown in reaction (4),

$$Sr^{2+}(H_2O)_x + Xe \rightarrow Sr^{2+}(H_2O)_{x-1} + H_2O + Xe. \quad (4)$$

At higher kinetic energies, water molecules are sequentially lost until the bare metal ion appears. For the CID of $Sr^{2+}(H_2O)_4$, $Sr^{2+}(H_2O)_5$, and $Sr^{2+}(H_2O)_6$, the energy range was not large enough to observe the Sr^{2+} ion with appreciable intensity. A proton transfer/charge separation process from the $Sr^{2+}(H_2O)_2$ complex, reaction (5), is observed in the CID of $Sr^{2+}(H_2O)_2$ and $Sr^{2+}(H_2O)_3$,

$$Sr^{2+}(H_2O)_2 + Xe \rightarrow SrOH^+ + H_3O^+ + Xe, \quad (5)$$

but no other complexes are observed to undergo such a process. The product cross sections of $SrOH^+$ and H_3O^+ ions have a higher apparent threshold than the $Sr^{2+}(H_2O)$ product cross section with amplitudes that are smaller by two orders of magnitude. These charge separated products could only be observed efficiently at Xe pressures somewhat higher than those normally used (~0.25 mTorr for $x=2$ and ~0.40 mTorr for $x=3$). No other products were observed besides those described above.

B. Comparison of CID cross sections for ions generated with ESI and DC/FT sources

In addition to the CID of $Sr^{2+}(H_2O)_x$ complexes generated by the ESI source, CID studies of $Sr^{2+}(H_2O)_x$ ions, where $x=1-6$, were carried out for ions generated with a DC/FT.[9] Intensities for $x=4-6$ were reasonably large and decreased appreciably for smaller complexes. Comparisons of the total CID cross sections obtained using these two sources are shown in Fig. 2 for $x=1-4$. Comparisons for $x=5$ and 6 can be found in supporting information, Fig. S1.[66] In general, the CID cross sections for ions generated with the ESI source are considerably cleaner than those generated with the DC/FT source and rise sharply from zero. For $x=1$, the DC/FT product cross section is shifted to lower kinetic energies with respect to the ESI product cross section, which indicates dissociation proceeds from $Sr^{2+}(H_2O)$ complexes that could not dissipate excess internal energy acquired in the association process forming the ions. Like $x=1$, the DC/FT total cross section for $x=2$ is shifted to lower energies with respect to the ESI cross section but also includes a low energy feature from 0.0 to 1.2 eV. Such low energy features may indicate the presence of a small population of high energy conformers within the ion beam. With only two water molecules complexed to Sr^{2+}, this high energy conformer can only correspond to a structure in which the second water molecule is located in the second solvent shell and hydrogen bonds to the inner shell water molecule. These low energy tails closely resemble features that can be purposely introduced using the in-source fragmentation technique.[22] For $x=3$, the low energy feature persists, but the DC/FT and ESI total cross sections are comparable from 1.3 to 5.0 eV. Assuming the low energy feature is attributed to a high energy conformer in the ion beam, the agreement in the two cross sections indicates that the low energy conformer in the ion beam has an internal energy distribution similar to that for ions generated with ESI. The DC/FT and ESI cross sections for the $Sr^{2+}(H_2O)_4$ complex are similar, Fig. 2, although the DC/FT cross section magnitude is about half that of the ESI cross section (a result that can probably be attributed to incomplete collection of product ions in the DC/FT data). For $x=5$ and 6, the DC/FT and ESI cross sections are comparable in magnitude but the former has low energy tails that could either be from hot ions or alternate conformations. Overall, these comparisons indicate that the ESI source generates $Sr^{2+}(H_2O)_x$ complexes consisting of single conformations that are well thermalized. The flow tube source, which generally has been found to produce well-thermalized singly charged ions,[29,30,46–49] is apparently limited in its ability to dissipate the association energies of doubly charged ions.

C. Thermochemical results

The total dissociation cross sections from ESI generated ions were modeled using Eqs. (1) and (2) for all $Sr^{2+}(H_2O)_x$ complexes. The total cross section is modeled because the overall shapes of the cross sections for reaction (4) are influenced by sequential dissociation of additional water molecules. The optimum modeling parameters obtained are listed in Table I and the models of Eq. (2) are compared to zero pressure-extrapolated cross sections in Fig. 3 for $Sr^{2+}(H_2O)_x$, where $x=1-6$. The model of Eq. (2) reproduces the experimental data well from threshold to 10.0, 7.0, 5.0, 4.0, 3.5, and 2.0 eV for $x=1-6$, respectively. For $Sr^{2+}(H_2O)-Sr^{2+}(H_2O)_6$, the kinetic shift between E_0 values modeled with and without consideration of lifetime effects [Eqs. (2) and (1), respectively] gradually increases from 0.00 to 0.17 eV. In Fig. 3, the solid lines represent the model of Eq. (2) convoluted over the kinetic and internal energy distribution of the reactants, whereas the dashed lines represent the model without kinetic energy broadening or internal energy of the reactants. The energy difference between these two lines is largely a measure of the internal energy of the reactant complex at 300 K. It can be seen that the internal energy of the $Sr^{2+}(H_2O)$ complex is small, but systematically increases for larger $Sr^{2+}(H_2O)_x$ complexes. This is attributable to the relatively floppy motions in such metal-ligand donor-acceptor bonding.

Downloaded 02 Dec 2010 to 155.97.11.184. Redistribution subject to AIP license or copyright; see http://jcp.aip.org/about/rights_and_permissions

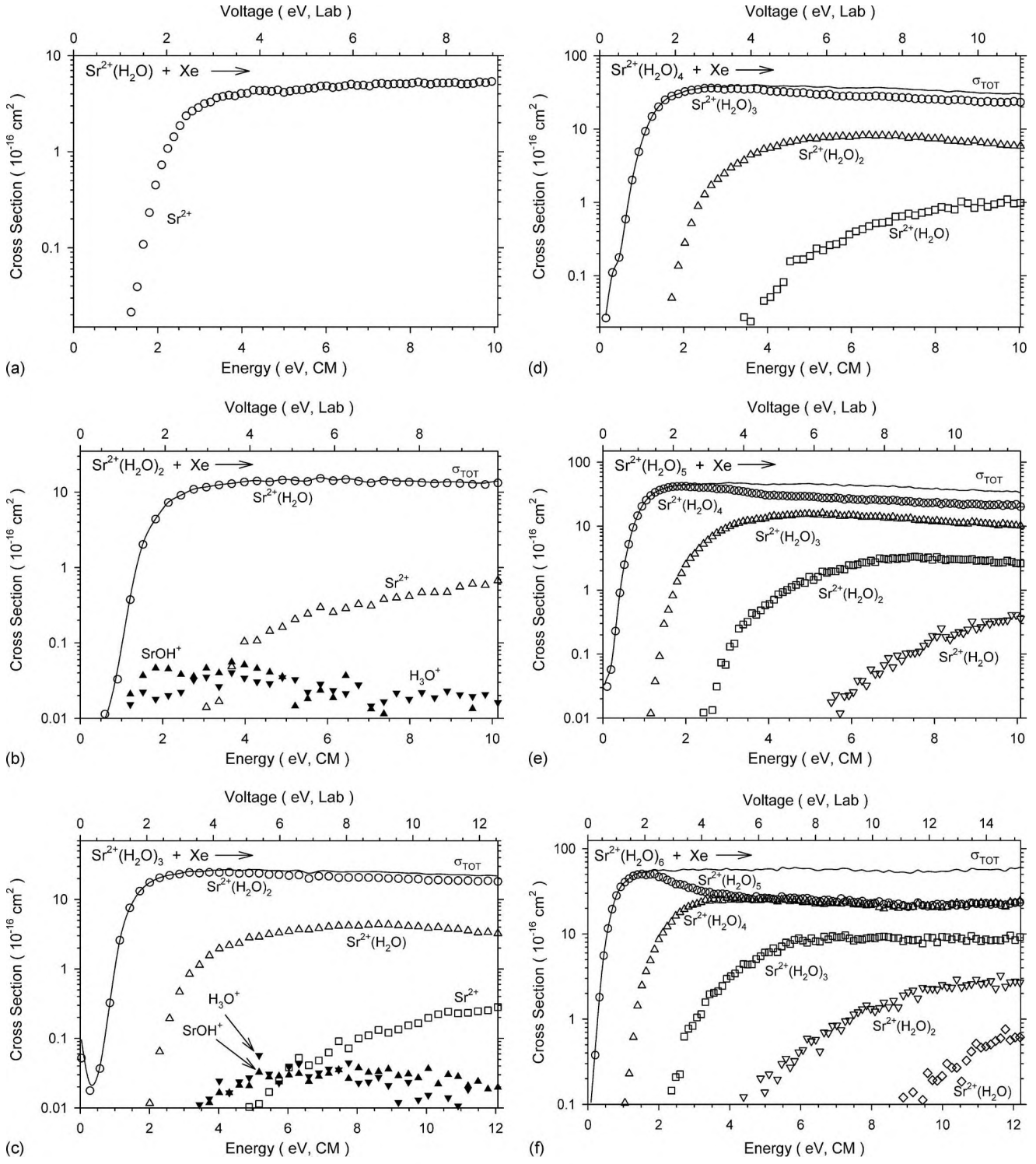

FIG. 1. Cross sections for collision-induced dissociation of $Sr^{2+}(H_2O)_x$ where $x=1-6$ (parts a–f, respectively) with xenon (~0.2 mTorr) as a function of kinetic energy in the CM frame (lower x-axis) and the laboratory frame voltage (upper x-axis). Xenon pressures for the CID of $Sr^{2+}(H_2O)_2$ and $Sr^{2+}(H_2O)_3$ were 0.25 and 0.40 mTorr, respectively.

D. Theoretical geometries of ground state $x=1-6$ structures

Geometry optimizations and frequency calculations were performed at B3LYP/HW*/6-311+G(d,p), B3LYP/SD/6-311+G(d,p), B3LYP/Def2TZVP, and BH&HLYP/Def2TZVPP levels of theory for $Sr^{2+}(H_2O)_x$ complexes. Structural details for $Sr^{2+}(H_2O)_x$ complexes at these three levels of theory are provided in Supporting Information, Tables SI–SIII.[66] Geometrical parameters do not change significantly between these three levels of theory, e.g., the Sr–O distances for a specific $Sr^{2+}(H_2O)_x$ complex are within 0.005 Å of one another at all levels. The structures

Downloaded 02 Dec 2010 to 155.97.11.184. Redistribution subject to AIP license or copyright; see http://jcp.aip.org/about/rights_and_permissions

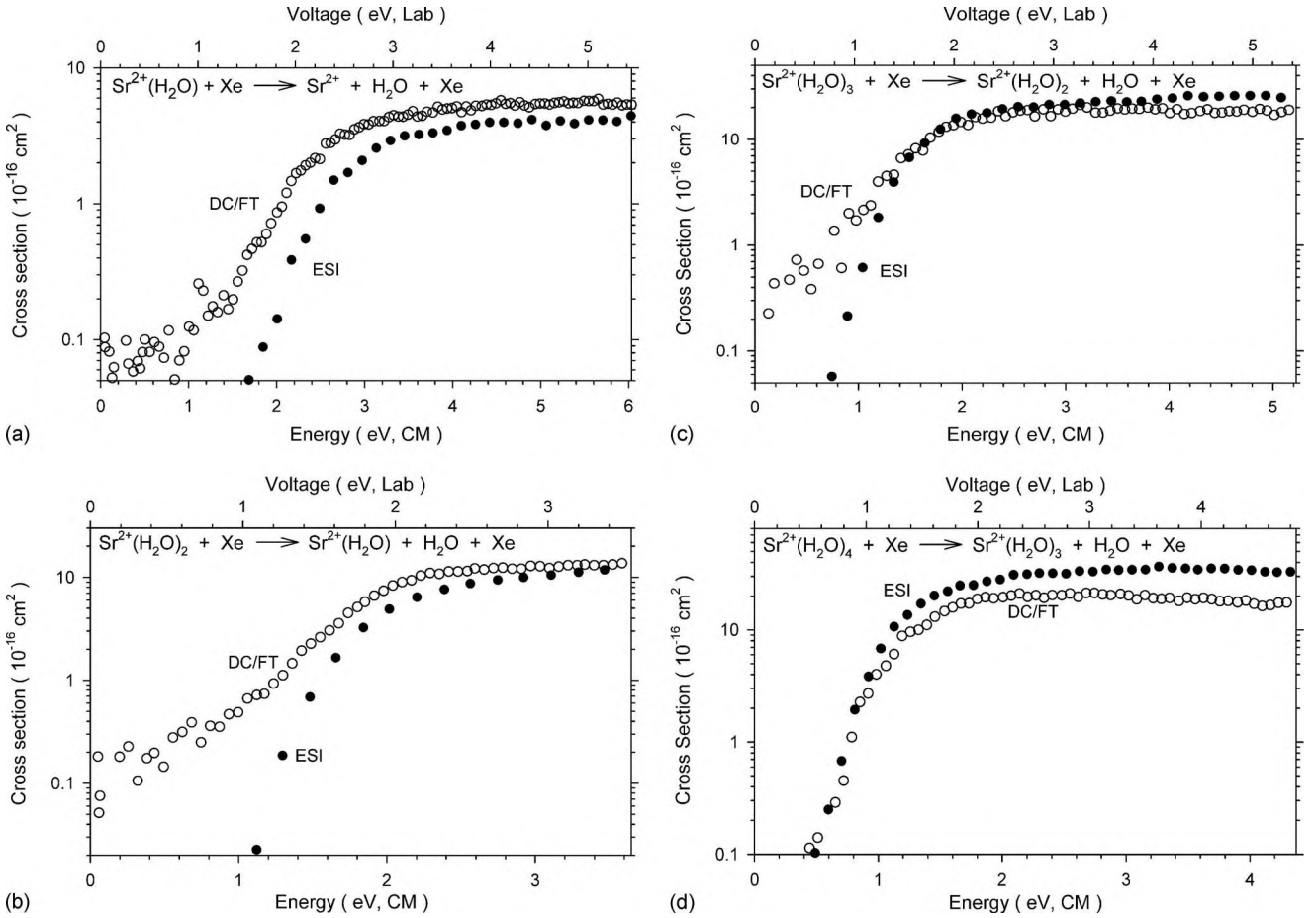

FIG. 2. Comparison of total cross sections for collision-induced dissociation of $Sr^{2+}(H_2O)_x$ where $x=1-4$ (parts a–d, respectively) with xenon for ions generated with the ESI source (solid symbols) and DC/FT source (open symbols).

for $x=1-6$ are shown in Fig. 4. In all cases, the dipole moment of the water ligand is directed toward the charged metal center. The Sr–O distances increase systematically by 0.033 ± 0.003 Å in going from $x=1$ to $x=6$, Fig. 4.

The $Sr^{2+}(H_2O)$ complex has C_{2v} symmetry as expected. The $Sr^{2+}(H_2O)_2$ complex has C_2 symmetry and is bent with an O–Sr–O angle between 117.0° and 119.5° depending on the level of theory. A bent geometry has also been calculated for the lowest energy $Ca^{2+}(H_2O)_2$ structure with O–Ca–O angles of 124.7° and 125.8° at the B3LYP/6-311+G(d,p) and MP2(full)/6-311+G(d,p) levels of theory, respectively,[7] whereas $Mg^{2+}(H_2O)_2$ complexes prefer a linear geometry with D_{2d} symmetry.[11–13] This structural difference is attributed to the larger core polarization of Sr^{2+} and Ca^{2+}, which compensates for the larger ligand-ligand repulsions in the bent geometry.[13] We find the lowest energy $Sr^{2+}(H_2O)_3$ complex has C_3 symmetry, whereas the lowest energy $Ca^{2+}(H_2O)_3$ and $Mg^{2+}(H_2O)_3$ complexes, adopt D_3 symmetries, in which all heavy atoms are located in the same plane.[11,13] In the C_3 geometry, the Sr^{2+} ion is located above a plane containing the oxygen atoms of the three water molecules with O–Sr–O angles between 113° and 118°. This

TABLE I. Parameters used to model the primary dissociation process for collision-induced dissociation of $Sr^{2+}(H_2O)_x$ ($x=1-6$). (Uncertainties are in parentheses.)

Reactant	Product	σ_0 [a]	n [a]	E_0 (PSL) (eV)[a]	E_0 (eV)[b]
$Sr^{2+}(H_2O)$	Sr^{2+}	8 (1)	0.86(0.05)	2.09(0.06)	2.09(0.06)
$Sr^{2+}(H_2O)_2$	$Sr^{2+}(H_2O)$	24 (2)	0.83(0.06)	1.78(0.05)	1.80(0.06)
$Sr^{2+}(H_2O)_3$	$Sr^{2+}(H_2O)_2$	41 (3)	0.86(0.06)	1.49(0.05)	1.53(0.06)
$Sr^{2+}(H_2O)_4$	$Sr^{2+}(H_2O)_3$	59 (3)	0.85(0.05)	1.29(0.04)	1.43(0.04)
$Sr^{2+}(H_2O)_5$	$Sr^{2+}(H_2O)_4$	72 (4)	0.77(0.06)	1.06(0.04)	1.21(0.05)
$Sr^{2+}(H_2O)_6$	$Sr^{2+}(H_2O)_5$	84 (3)	0.79(0.05)	0.97(0.03)	1.14(0.04)

[a]Parameters from modeling with Eq. (2), where lifetime effects are included.
[b]Parameters from modeling with Eq. (1), which excludes lifetime effects.

Downloaded 02 Dec 2010 to 155.97.11.184. Redistribution subject to AIP license or copyright; see http://jcp.aip.org/about/rights_and_permissions

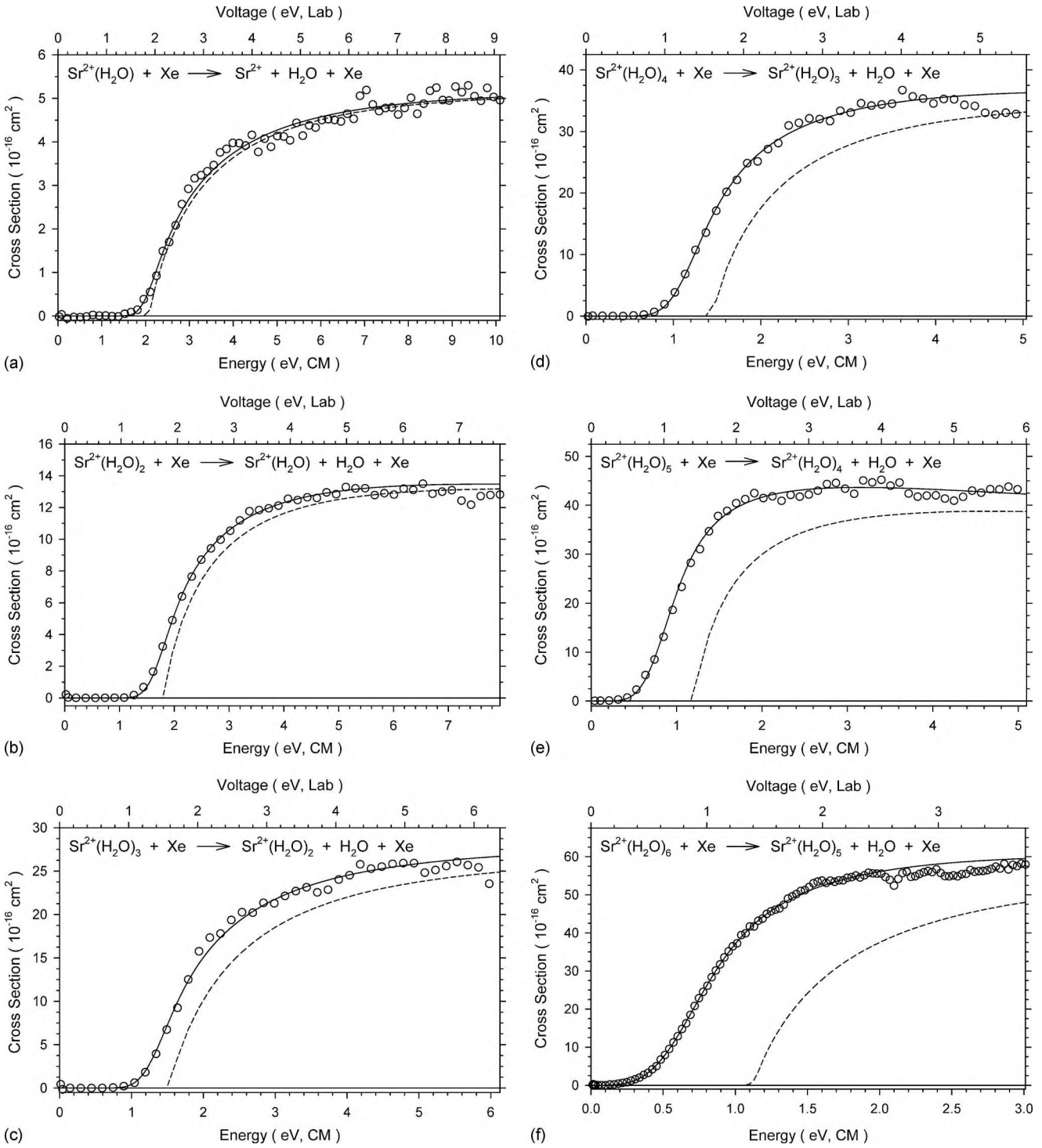

FIG. 3. Zero pressure extrapolated cross sections for collision-induced dissociation of $Sr^{2+}(H_2O)_x$ where $x=1-6$ (parts a–f, respectively) with xenon in the threshold region as a function of kinetic energy in the CM frame (lower x-axis) and the laboratory frame voltage (upper x-axis). The solid lines show the best fit to the data using the model of Eq. (2) convoluted over the neutral and ion kinetic and internal energy distributions. The dashed lines show the model cross sections in the absence of experimental kinetic energy broadening for reactions with an internal energy of 0 K.

pyramidal structure has also been attributed to the larger core polarization of Sr^{2+}.[13] The structures of $Sr^{2+}(H_2O)_4$, $Sr^{2+}(H_2O)_5$, and $Sr^{2+}(H_2O)_6$ have S_4, C_{2v}, and T_h symmetries and geometries similar to their calcium analogs.[7] In all cases, ligands are placed to minimize ligand-ligand repulsion but also to take advantage of weak hydrogen bonding between adjacent ligands.

E. Conversion from 0 to 298 K

$\Delta H_{298}-\Delta H_0$ and $T\Delta S_{298}$ values, Table II, are calculated with a rigid rotor/harmonic oscillator approximation using the vibrational frequencies and rotational constants calculated at the B3LYP/HW*/6-311+G(d,p) level of theory. The uncertainties for these values are found by scaling the vibrational frequencies up and down by 10%. These conver-

Downloaded 02 Dec 2010 to 155.97.11.184. Redistribution subject to AIP license or copyright; see http://jcp.aip.org/about/rights_and_permissions

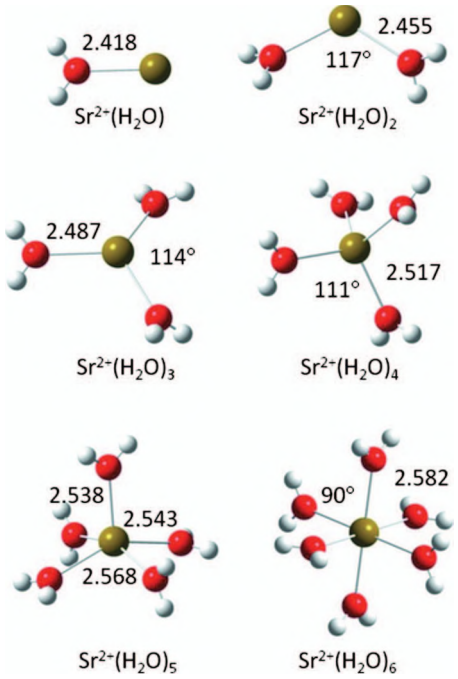

FIG. 4. Structures for $Sr^{2+}(H_2O)_x$, where $x=1-6$. Bond lengths (angstrom) and bond angles (degrees) shown are calculated at the B3LYP/Def2TZVP level.

sion factors are used to determine the ΔH_{298} and ΔG_{298} values listed in Table III, which are used for comparison to available literature results and calculated theoretical values.

F. Theoretical bond enthalpies

Theoretical bond enthalpies for losing a single water molecule from all $Sr^{2+}(H_2O)_x$ complexes are listed in Table III. These enthalpies include ZPE and thermal corrections to 298 K both with and without cp corrections. Single point energies were calculated at the B3LYP, B3P86, MP2(full), and M06 levels with HW*, SD, and Def2TZVPP basis sets from geometry optimizations using B3LYP/HW*/6-311+G(d,p), B3LYP/SD/6-311+G(d,p), and B3LYP/Def2TZVP levels of theory. Regardless of the basis set treatment, the B3LYP and B3P86 single point calculations produce almost identical binding enthalpies, differing by no more than 2 kJ/mol. MP2(full) results provide lower binding enthalpies for $x=1-4$ for HW* (by 3–11 kJ/mol) and $x=1-3$ for SD (3–11 kJ/mol) and Def2TZVPP (3–9 kJ/mol) basis sets with respect to B3LYP single point energies, but higher enthalpies by 4–8 kJ/mol for $x=5$ and 6 for all basis sets. For $x=1-4$, the M06 energies are 1–4 kJ/mol higher, 0–1 kJ/mol higher, and 1–2 lower than B3LYP energies calculated with the HW*, SD, and Def2TZVPP basis sets, respectively. The M06 energies for $x=5$ and 6 are most similar to the MP2(full) energies. Cp corrections for density functional theory (DFT) (B3LYP, B3P86, and M06) calculations are 1–2 kJ/mol for the HW* or SD basis sets and 3–5 kJ/mol for the Def2TZVPP basis set, whereas for MP2(full) calculations, they are 5–12, 5–9, and 6–10 kJ/mol for the HW*, SD, and Def2TZVPP basis set treatments.

Overall, B3LYP and B3P86 energies calculated with the HW* or SD treatment and all M06 energies are slightly higher than the B3LYP/Def2TZVPP energies, but within 2–3 kJ/mol when cp corrections are included. MP2(full) results are 5–6 kJ/mol above those for B3LYP and B3P86 calculations and change little when cp corrections are not included, Table III.

G. Charge separation channel

We have previously defined the critical size for a $M^{2+}(H_2O)_x$ system as the complex size (x) at which charge separation becomes the lower energy pathway compared to simple ligand loss.[22] $Sr^{2+}(H_2O)_2$ is the only complex that undergoes charge separation, leading to the $SrOH^+$ and H_3O^+ products. The apparent thresholds of the charge separation product cross sections lie above the apparent threshold for the $Sr^{2+}(H_2O)$ product cross sections, Figs. 1(b) and 1(c). We attempted to analyze the cross sections for this process using Eq. (2), but because they are only observed at high Xe pressures, no reliable zero pressure extrapolated cross sections suitable for thermodynamic analysis could be obtained.

The theoretical reaction coordinate for charge separation from $Sr^{2+}(H_2O)_2$ is shown in Fig. 5 as calculated at the B3LYP/Def2TZVPP level of theory. Charge separation involves transferring a water molecule from the inner solvent shell to the second solvent shell, where it binds through a single hydrogen bond. As the products separate, a proton is transferred to the second solvent shell water molecule, thereby forming two singly charged ions that separate from one another over a large Coulombic barrier.[67] Table IV provides relative energies of the TSs, intermediates, and prod-

TABLE II. Conversion between 0 K binding energies for H_2O loss from $Sr^{2+}(H_2O)_x$ ($x=1-6$) to enthalpies and free energies at 298 K in kJ/mol. (Uncertainties are in parentheses.)

Complex	ΔH_0 [a]	$\Delta H_{298}-\Delta H_0$ [b]	ΔH_{298}	$T\Delta S_{298}$ [b]	ΔG_{298}
$Sr^{2+}(H_2O)$	201.3(6.1)	4.3(0.2)	205.6(6.1)	28.5(0.5)	177.1(6.1)
$Sr^{2+}(H_2O)_2$	172.1(4.6)	1.0(0.2)	173.1(4.7)	22.8(1.2)	150.3(4.8)
$Sr^{2+}(H_2O)_3$	144.2(5.1)	1.5(0.2)	145.7(5.1)	36.3(1.3)	109.4(5.2)
$Sr^{2+}(H_2O)_4$	124.2(3.6)	1.0(0.2)	125.2(3.6)	33.1(1.3)	92.1(3.9)
$Sr^{2+}(H_2O)_5$	102.6(3.5)	1.8(0.3)	104.4(3.5)	41.5(1.3)	62.9(3.7)
$Sr^{2+}(H_2O)_6$	93.6(2.7)	1.0(0.3)	94.7(2.7)	40.2(1.3)	54.5(3.0)

[a]Experimental values from this work (Table I).
[b]Values were calculated using standard formulae and molecular constants calculated at the B3LYP/HW*/6-311+G(d,p) level. Uncertainties were determined by scaling the vibrational frequencies up and down by 10%.

Downloaded 02 Dec 2010 to 155.97.11.184. Redistribution subject to AIP license or copyright; see http://jcp.aip.org/about/rights_and_permissions

TABLE III. Experimental and theoretical 298 K bond enthalpies for H_2O loss from ground state $Sr^{2+}(H_2O)_x$ ($x=1-6$) in kJ/mol.

Experiment		$x=1$	2	3	4	5	6	
This work		206 ± 6	173 ± 5	146 ± 5	125 ± 4	104 ± 4	95 ± 3	
HPMS[a]							95 ± 4	
BIRD[b]						100 ± 4	87 ± 4	
Geometry[c]	Single point[d]	$x=1$	2	3	4	5	6	MAD[e]
B3LYP/HW*/6-311+G(d,p)	M06	195 (196)	167 (169)	148 (150)	131 (133)	111 (113)	100 (102)	6 ± 3 (7 ± 2)
	B3LYP	191 (192)	165 (166)	146 (148)	130 (131)	104 (106)	93 (95)	5 ± 5 (5 ± 5)
	B3P86	194 (195)	166 (167)	147 (149)	130 (132)	104 (106)	93 (95)	5 ± 4 (5 ± 4)
	MP2(full)	180 (186)	158 (163)	142 (148)	127 (134)	108 (116)	98 (109)	9 ± 9 (11 ± 6)
B3LYP/SD/6-311+G(d,p)	M06	195 (196)	167 (169)	148 (150)	130 (132)	111 (113)	101 (103)	6 ± 3 (7 ± 2)
	B3LYP	193 (193)	166 (167)	147 (149)	130 (132)	104 (106)	93 (95)	5 ± 5 (5 ± 4)
	B3P86	194 (195)	167 (168)	148 (150)	130 (132)	104 (106)	93 (95)	5 ± 4 (5 ± 4)
	MP2(full)	183 (188)	160 (166)	144 (151)	130 (137)	109 (117)	101 (110)	9 ± 8 (12 ± 5)
B3LYP/Def2TZVP	M06	195 (198)	169 (172)	148 (151)	130 (133)	111 (114)	101 (105)	6 ± 3 (7 ± 4)
	B3LYP	197 (200)	171 (175)	150 (154)	132 (136)	105 (110)	94 (99)	4 ± 3 (6 ± 3)
	B3P86	197 (200)	171 (174)	149 (153)	131 (135)	105 (109)	93 (97)	4 ± 3 (5 ± 3)
	MP2(full)	188 (194)	166 (172)	147 (154)	132 (139)	110 (118)	100 (110)	8 ± 6 (11 ± 5)
BH&HLYP/Def2TZVPP	BH&HLYP	199 (202)	166 (166)	151 (151)	132 (132)	105 (106)	95 (95)	4 ± 3 (4 ± 3)
GI[f]		198	174	156	141	116	106	10 ± 5
Klobukowski[g]		(181)	(166)	(154)	(137)			(13 ± 8)
BSP[h]		(187)	(168)	(152)				(10 ± 8)
KS[i]		(198)	(179)					(6 ± 1)

[a]Values from Ref. 3.
[b]Values from Ref. 5.
[c]Level of theory for geometry optimization.
[d]Basis sets for single point energies are HW*/6-311+G(2d,2p), SD/6-311+G(2d,2p), or Def2TZVPP. Single point energies in parentheses do not include cp corrections.
[e]MADs from experimental binding enthalpies.
[f]Theoretical results from Ref. 10.
[g]Theoretical results from Ref. 11. Values corrected to 298 K.
[h]Theoretical results from Ref. 12. Values corrected to 298 K.
[i]Theoretical results from Ref. 13. Values corrected to 298 K.

ucts for the charge separation and water loss pathways from $Sr^{2+}(H_2O)_2$ calculated at the B3LYP and MP2(full) levels with the HW*, SD, and Def2TZVPP basis sets. The calculations indicate that ~60 kJ/mol of energy is required to transfer a water molecule into the second solvent shell (TS1) and that this alternate structure (INT) is less stable than the bisligated ground state by 56–60 kJ/mol. The relative B3LYP energies predict that charge separation over TS2 is favored over water loss by 0–19 kJ/mol for all three basis sets, whereas MP2(full) results predict water loss is the lower energy pathway by 0–24 kJ/mol. Overall, the $Sr^{2+}(H_2O)_2$ ground state is calculated to be metastable at the B3LYP level of theory by 13–34 kJ/mol, whereas MP2(full) calculations yield higher relative energies of −14 to +13 kJ/mol, Table IV.

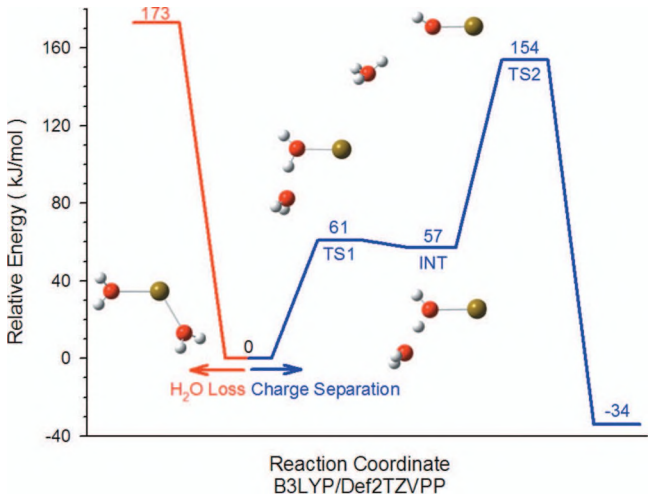

FIG. 5. Reaction coordinates for water loss and charge separation pathways for $Sr^{2+}(H_2O)_2$ calculated at the B3LYP/Def2TZVPP level of theory including zero-point energy corrections.

TABLE IV. Relative 0 K energies of TSs, intermediates, and products for charge separation and water loss from $Sr^{2+}(H_2O)_2$. [B3LYP energies are in roman text. MP2(full) energies are in bold text.]

Complex	HW* [a]	SD[b]	Def2TZVPP[c]
$Sr^{2+}(H_2O)+H_2O$	165, **162**	166, **165**	173, **170**
$Sr^{2+}(H_2O)_2$	0, **0**	0, **0**	0, **0**
TS1	60, **59**	60, **61**	61, **60**
INT	56, **58**	57, **60**	57, **58**
TS2	165, **186**	160, **181**	154, **170**
$SrOH^+ + H_3O^+$	−13, **13**	−24, **4**	−34, **−14**

[a]Single point energies calculated with the HW*/6-311+G(2d,2p) basis set using B3LYP/HW*/6-311+G(d,p) geometries and ZPE corrections.
[b]Single point energies calculated with the SD/6-311+G(2d,2p) basis set using B3LYP/SD/6-311+G(d,p) geometries and ZPE corrections.
[c]Single point energies calculated with the Def2TZVPP basis set using B3LYP/Def2TZVP geometries and ZPE corrections.

Downloaded 02 Dec 2010 to 155.97.11.184. Redistribution subject to AIP license or copyright; see http://jcp.aip.org/about/rights_and_permissions

Previous work has assigned a critical size of $x=2$ for hydrated strontium dications on the basis that this was the only complex to exhibit charge separation.[68] Using our thermodynamic criterion for defining the critical size, the B3LYP calculations indicate that the critical size complex for the $Sr^{2+}(H_2O)_x$ system is $x=2$, whereas the MP2(full) calculations suggest there is no critical size for strontium hydrates. In this regard, the apparent relative thresholds for reactions (4) and (5) agree better with the MP2(full) results, although the observation of the entropically disfavored charge separation reaction indicates its threshold must be close to that for reaction (4), in agreement with theory. The relative magnitudes of the water loss and charge separation cross sections, Fig. 1, are consistent with our ability to form the $Sr^{2+}(H_2O)$ complex in the ESI source by fragmentation of the larger $Sr^{2+}(H_2O)_2$ complex.

H. Literature calculations

Table III includes results from four theoretical studies in the literature. Glendening and Feller[11] calculated geometries and single point energies for $Sr^{2+}(H_2O)_x$, where $x=1-6$, using the MP2(full)/6-31+G(d)//RHF/6-31+G(d) level of theory. The Hay–Wadt ECP and basis set described the Sr^{2+} ion and correlation of the 1s electrons of the oxygen atoms was neglected in the frozen-core MP2 treatment. Klobukowski[12] calculated Hartree–Fock binding energies for $x=1-4$ using the Hay–Wadt ECP and basis set for the Sr^{2+} ion and Huzinaga basis sets of triple-zeta quality for the water molecules. Bauschlicher and co-workers[13] also calculated Hartree–Fock binding energies for $x=1-3$ utilizing the Hay–Wadt ECP and basis set for Sr^{2+}, while treating the water molecules with Dunning basis sets of triple zeta plus polarization quality. Finally, Kaupp and Schleyer[14] calculated MP2 geometries and binding energies for $Sr^{2+}(H_2O)$ and $Sr^{2+}(H_2O)_2$ utilizing a ten valence-electron quasirelativistic energy-adjusted pseudopotential for Sr^{2+}, single-electron-fit pseudopotentials for oxygen atoms, and a Dunning and Hay basis for hydrogen atoms. In all cases, the $Sr^{2+}(H_2O)_x$ optimized geometries of these literature studies are similar to those presented in Fig. 4, except that Klobukowski considered only quasilinear D_{2d} and D_{2h} geometries for $x=2$. Glendening and Feller included ZPE, thermal, and BSSE corrections in their calculations of the sequential hydration energies, but the latter three studies did not. Therefore, these literature values are corrected for ZPE and thermal corrections using values calculated here at the B3LYP/HW*/6-311+G(d,p) level to facilitate comparisons discussed below. The corrections applied here are 10 kJ/mol for $Sr^{2+}(H_2O)$ and 7 kJ/mol for the $Sr^{2+}(H_2O)_2$, $Sr^{2+}(H_2O)_3$, and $Sr^{2+}(H_2O)_4$ complexes.

IV. DISCUSSION

A. Comparison between experimental and literature experimental values

Available results from other experimental studies found in the literature are included in Table III and Fig. 6. For $x=6$, our experimental value is identical to the result from HPMS studies of Kebarle and co-workers.[3] For $x=5$ and 6, our results are 4 and 8 kJ/mol higher than those from BIRD studies of Williams and co-workers.[5] The latter difference is slightly outside the range of the combined uncertainties.

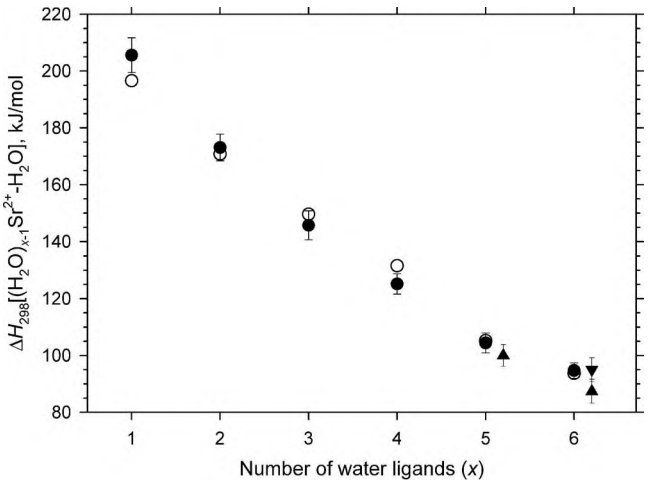

FIG. 6. Comparison of present experimental (solid circles) and theoretical B3LYP/Def2TZVPP (open circles) bond enthalpies at 298 K. HPMS results from Ref. 3 (solid down triangles) and BIRD results from Ref. 5 (solid up triangles) are also included.

B. Comparison between present experiment and theory

The present theoretical results of Table III can be compared to the experimental binding enthalpies by determining the mean absolute deviations (MADs). Our experimental binding enthalpies agree best with the cp-corrected B3LYP/Def2TZVPP energies with a MAD of 4 ± 3 kJ/mol, Fig. 6, whereas a MAD of 6 ± 3 kJ/mol is found for B3LYP/Def2TZVPP energies without cp corrections. MADs for the B3LYP/HW*, B3P86/HW*, B3LYP/SD, and B3P86/SD energies are slightly higher at 5 ± 5, 5 ± 4, 5 ± 5, and 5 ± 4 kJ/mol. M06 energies have MADs of 6 ± 3 kJ/mol with respect to the experimental binding enthalpies. MP2(full) energies have MADs that are consistently 4 kJ/mol higher than the MADs for B3LYP energies for a specific basis set treatment. For B3LYP and B3P86 calculations with the HW* and SD basis set treatments, the MADs with and without cp corrections do not significantly change because the corrections are small (1–2 kJ/mol). The MADs from the B3LYP and B3P86 levels with the Def2TZVPP basis set decrease slightly (by 1–2 kJ/mol) when cp corrections are included because the deviations for $x=3-6$ are reduced. A more noticeable difference is seen for the MP2(full) binding enthalpies, which have larger BSSEs (5–12 kJ/mol) and lead to a MAD decrease of 2–3 kJ/mol when the cp corrections are included.

The most significant difference between the theoretical calculations and experimental results is usually for the $Sr^{2+}(H_2O)$ complex. MADs would decrease by 0–4 kJ/mol for all calculations if the deviations for the monohydrate binding energy were excluded. Regardless of the chosen ECP, DFT and MP2(full) energies predict a value 4–14 and 12–25 kJ/mol lower, respectively, than the experimental hydration energy of 206 ± 6 kJ/mol. A possible explanation for

Downloaded 02 Dec 2010 to 155.97.11.184. Redistribution subject to AIP license or copyright; see http://jcp.aip.org/about/rights_and_permissions

this is that core polarization of the Sr is not adequately handled for this complex, in part because an ECP is used. If such polarization were included properly, the water molecule could pull closer to the metal center, thereby resulting in a larger calculated binding energy. Experimental binding energies for $x=2-6$ are reproduced quite well by B3LYP and B3P86 energies for all basis set treatments. B3LYP and B3P86 energies with the HW* and SD basis set treatments are 6–8 kJ/mol lower than the experimental binding enthalpy of 173 ± 5 kJ/mol for $Sr^{2+}(H_2O)_2$, whereas the Def2TZVPP energies fall within experimental uncertainty. For $Sr^{2+}(H_2O)_4$, the experimental binding enthalpy of 125 ± 4 kJ/mol is slightly below the 130–132 kJ/mol range predicted by most levels of theory, whereas the experimental results for $x=3$, 5, and 6 agree with the B3LYP and B3P86 calculations regardless of the basis set treatment. Overall, the levels of theory giving the best agreement with experiment are DFT approaches (excluding M06) using the Def2TZVPP basis set.

C. Comparison between experimental and literature theoretical values

The results from four theoretical studies are also provided in Table III. Cp-corrected MP2 single point energies calculated by Glendening and Feller[11] have a MAD of 10 ± 5 kJ/mol with respect to our experimental binding energies. Their calculated binding energies agree reasonably well with our experimental results for $x=1$ and 2, but the binding energies for $x=3-6$ are systematically higher by 10–16 kJ/mol. This is similar to previous results on the analogous calcium complexes.[7] There, our B3LYP/6-311+G(2d,2p)//B3LYP/6-311+G(d,p) binding enthalpies were comparable to those calculated by Glendening and Feller for $x=1$ and 2, but their values were higher than ours by 7–13 kJ/mol for $x=3-6$. There, we suggested that these bond energies would decrease if electron correlation was included in the geometry optimization and if the basis sets in the single point energies included extra polarization functions. 298 K binding enthalpies for $Sr^{2+}(H_2O)_x$ from Klobukowski,[12] Bauschlicher and co-workers (BSP),[13] and Kaupp and Schleyer (KS)[14] have MADs of 13 ± 8, 10 ± 8, and 6 ± 1 kJ/mol with respect to our experimental results, respectively. Compared to our experimental results, the binding enthalpies for $x=1$ and 2 of Klobukowski are smaller by 25 and 7 kJ/mol, but larger for $x=3$ and 4 by 10 and 16 kJ/mol, respectively. BSP binding enthalpies are similar to Klobukowski's results for $x=2$ and 3, differing by only 2 kJ/mol, whereas the binding for $x=1$ is now 6 kJ/mol higher. For KS, the values for $x=1$ and 2 are in good agreement with our experimental results. More useful comparisons could be made here if these latter three theoretical studies determined binding enthalpies for all of the inner shell complexes and included corrections for BSSEs.

V. CONCLUSIONS

The kinetic energy dependent cross sections for $Sr^{2+}(H_2O)_x$, where $x=1-6$, are determined by TCID using a guided ion beam mass spectrometer equipped with an ESI source. Qualitative comparisons between the CID cross sections for $Sr^{2+}(H_2O)_x$ ions generated with the ESI source and DC/FT source indicate that the ESI source produces ions that are better thermalized than ions generated with the flow tube source. The electrospray source produces an initial distribution of $Sr^{2+}(H_2O)_x$ complexes where $x=6-9$. Smaller $Sr^{2+}(H_2O)_x$ complexes, where $x=1-5$, are accessed with a recently developed in-source fragmentation technique that takes place in the high pressure region of the rf-only hexapole ion guide.[22] This source can successfully generate reactant complexes in which all water molecules are bound directly to the ion. The dominant process taking place in all systems is the loss of a single water molecule. A charge separation process is observed once the $Sr^{2+}(H_2O)_2$ complex is reached, but the product cross sections for charge separation have magnitudes that are significantly smaller than those for the $Sr^{2+}(H_2O)$ product cross section. Theoretical calculations indicate that water loss and the charge separation process are similar energetically, but the latter process is entropically disfavored. This explains why the formation of the $Sr^{2+}(H_2O)$ complex is possible with the in-source fragmentation technique.

The present work determines the first experimental hydration energies for $Sr^{2+}(H_2O)$ to $Sr^{2+}(H_2O)_4$. Our experimental results for $Sr^{2+}(H_2O)_5$ and $Sr^{2+}(H_2O)_6$ agree well with available thermochemistry from HPMS and BIRD studies.[3,5] We find that our experimental hydration energies are in very good agreement with binding enthalpies calculated at the B3LYP, B3P86, and BH&HLYP levels of theory with the Def2TZVPP basis set, although the HW*/6-311+G(2d,2p) and SD/6-311+G(2d,2p) basis sets are only marginally worse. For $Sr^{2+}(H_2O)$ and $Sr^{2+}(H_2O)_2$, the Def2TZVPP basis set calculates binding enthalpies that are slightly higher than those utilizing the HW* or SD treatment and are in better agreement with experimental binding enthalpies. These theoretical results are also in accord with lower level theoretical results in the literature. The good agreement between theoretical and experimental binding energies provides confidence that the TCID approach provides accurate thermodynamic information for multiply charged ions and that the ESI source produces thermalized ions of multiply charged complexes such as $M^{2+}(H_2O)_x$.

ACKNOWLEDGMENTS

Funding for this work was provided by the National Science Foundation under Grant No. 0748790. All theoretical calculations were performed using the Arches Cluster at the University of Utah's Center for High Performance Computing (CHPC). D.R.C. would like to thank Anita Orendt at the CHPC for assistance in setting up the M06 calculations in NWChem.

[1] C. M. Whitehouse. R. N. Dreyer. M. Yamashita. and J. B. Fenn. Anal. Chem. 57. 675 (1985).
[2] M. Yamashita and J. B. Fenn. J. Phys. Chem. 88. 4451 (1984).
[3] M. Peschke. A. T. Blades. and P. Kebarle. J. Phys. Chem. A 102. 9978 (1998).
[4] A. T. Blades. P. Jayaweera. M. G. Ikonomou. and P. Kebarle. J. Chem. Phys. 92. 5900 (1990).
[5] S. E. Rodriguez-Cruz. R. A. Jockusch. and E. R. Williams. J. Am. Chem.

Downloaded 02 Dec 2010 to 155.97.11.184. Redistribution subject to AIP license or copyright; see http://jcp.aip.org/about/rights_and_permissions

Soc. **121**. 8898 (1999).
[6] R. L. Wong, K. Paech, and E. R. Williams, Int. J. Mass Spectrom. **232**, 59 (2004).
[7] D. R. Carl, R. M. Moision, and P. B. Armentrout, Int. J. Mass Spectrom. **265**, 308 (2007).
[8] K. M. Ervin and P. B. Armentrout, J. Chem. Phys. **83**, 166 (1985).
[9] R. H. Schultz and P. B. Armentrout, Int. J. Mass Spectrom. Ion Process. **107**, 29 (1991).
[10] NIST Chemistry WebBook, NIST Standard Reference Database Number 69, Vol. (http://webbook.nist.gov), edited by P. J. Linstrom and W. G. Mallard (National Institute of Standards and Technology, Gaithersburg MD, 20899, 2003).
[11] E. D. Glendening and D. Feller, J. Phys. Chem. **100**, 4790 (1996).
[12] M. Klobukowski, Can. J. Chem. **70**, 589 (1992).
[13] C. W. Bauschlicher, M. Sodupe, and H. Partridge, J. Chem. Phys. **96**, 4453 (1992).
[14] M. Kaupp and P. V. Schleyer, J. Phys. Chem. **96**, 7316 (1992).
[15] F. Muntean and P. B. Armentrout, J. Chem. Phys. **115**, 1213 (2001).
[16] J. B. Fenn, M. Mann, C. K. Meng, S. F. Wong, and C. M. Whitehouse, Mass Spectrom. Rev. **9**, 37 (1990).
[17] R. M. Moision and P. B. Armentrout, J. Am. Soc. Mass Spectrom. **18**, 1124 (2007).
[18] T. Kim, A. V. Tolmachev, R. Harkewicz, D. C. Prior, G. Anderson, H. R. Udseth, and R. D. Smith, Anal. Chem. **72**, 2247 (2000).
[19] A. L. Heaton, R. M. Moision, and P. B. Armentrout, J. Phys. Chem. A **112**, 3319 (2008).
[20] A. L. Heaton and P. B. Armentrout, J. Phys. Chem. A **112**, 10156 (2008).
[21] A. L. Heaton and P. B. Armentrout, J. Phys. Chem. B **112**, 12056 (2008).
[22] D. R. Carl, R. M. Moision, and P. B. Armentrout, J. Am. Soc. Mass Spectrom. **20**, 2312 (2009).
[23] R. H. Schultz, K. C. Crellin, and P. B. Armentrout, J. Am. Chem. Soc. **113**, 8590 (1991).
[24] E. R. Fisher and P. B. Armentrout, J. Chem. Phys. **94**, 1150 (1991).
[25] E. R. Fisher, B. L. Kickel, and P. B. Armentrout, J. Chem. Phys. **97**, 4859 (1992).
[26] M. T. Rodgers and P. B. Armentrout, J. Phys. Chem. A **101**, 1238 (1997).
[27] M. T. Rodgers and P. B. Armentrout, Int. J. Mass Spectrom. **185–187**, 359 (1999).
[28] M. T. Rodgers and P. B. Armentrout, J. Phys. Chem. A **103**, 4955 (1999).
[29] R. M. Moision and P. B. Armentrout, Phys. Chem. Chem. Phys. **6**, 2588 (2004).
[30] R. M. Moision and P. B. Armentrout, J. Phys. Chem. A **110**, 3933 (2006).
[31] D. Gerlich, Adv. Chem. Phys. **82**, 1 (1992).
[32] E. Teloy and D. Gerlich, Chem. Phys. **4**, 417 (1974).
[33] N. Aristov and P. B. Armentrout, J. Phys. Chem. **90**, 5135 (1986).
[34] N. F. Dalleska, K. Honma, L. S. Sunderlin, and P. B. Armentrout, J. Am. Chem. Soc. **116**, 3519 (1994).
[35] N. R. Daly, Rev. Sci. Instrum. **31**, 264 (1960).
[36] T. S. Beyer and D. F. Swinehart, Commun. ACM **16**, 379 (1973).
[37] S. E. Stein and B. S. Rabinovich, Chem. Phys. Lett. **49**, 183 (1977).
[38] S. E. Stein and B. S. Rabinovich, J. Chem. Phys. **58**, 2438 (1973).
[39] R. G. Gilbert and S. C. Smith, *Theory of Unimolecular and Recombination Reactions* (Blackwell Scientific, London, 1990).
[40] D. A. Hales, L. Lian, and P. B. Armentrout, Int. J. Mass Spectrom. Ion Process. **102**, 269 (1990).
[41] K. A. Holbrook, M. J. Pilling, and S. H. Robertson, *Unimolecular Reactions*, 2nd ed. (Wiley, New York, 1996).
[42] D. G. Truhlar, B. C. Garrett, and S. J. Klippenstein, J. Phys. Chem. **100**, 12771 (1996).
[43] S. K. Loh, D. A. Hales, L. Lian, and P. B. Armentrout, J. Chem. Phys. **90**, 5466 (1989).
[44] F. A. Khan, D. E. Clemmer, R. H. Schultz, and P. B. Armentrout, J. Phys. Chem. **97**, 7978 (1993).
[45] M. T. Rodgers, K. M. Ervin, and P. B. Armentrout, J. Chem. Phys. **106**, 4499 (1997).
[46] C. Iceman and P. B. Armentrout, Int. J. Mass Spectrom. **222**, 329 (2003).
[47] M. T. Rodgers and P. B. Armentrout, J. Am. Chem. Soc. **122**, 8548 (2000).
[48] J. C. Amicangelo and P. B. Armentrout, J. Phys. Chem. A **104**, 11420 (2000).
[49] R. M. Moision and P. B. Armentrout, J. Phys. Chem. A **106**, 10350 (2002).
[50] P. B. Armentrout and J. Simons, J. Am. Chem. Soc. **114**, 8627 (1992).
[51] E. V. Waage and B. S. Rabinovitch, Chem. Rev. **70**, 377 (1970).
[52] M. J. Frisch, G. W. Trucks, H. B. Schlegel *et al.*, Gaussian, Inc., Pittsburgh, PA, 2003.
[53] A. D. Becke, J. Chem. Phys. **98**, 5648 (1993).
[54] C. Lee, W. Yang, and R. G. Parr, Phys. Rev. B **37**, 785 (1988).
[55] P. J. Hay and W. R. Wadt, J. Chem. Phys. **82**, 299 (1985).
[56] M. Kaupp, P. R. Schleyer, H. Stoll, and J. Preuss, J. Chem. Phys. **94**, 1360 (1991).
[57] F. Weigend and R. Ahlrichs, Phys. Chem. Chem. Phys. **7**, 3297 (2005).
[58] C. W. Bauschlicher, Jr. and H. Partridge, J. Chem. Phys. **103**, 1788 (1995).
[59] J. P. Perdew, Phys. Rev. B **33**, 8822 (1986).
[60] C. Møller and M. S. Plesset, Phys. Rev. **46**, 618 (1934).
[61] Y. Zhao and D. G. Truhlar, Theor. Chem. Acc. **120**, 215 (2008).
[62] E. J. Bylaska, W. A. d. Jong, N. Govind, K. Kowalski, T. P. Straatsma, M. Valiev, D. Wang, E. Apra, T. L. Windus, J. Hammond, P. Nichols, S. Hirata, M. T. Hackler, Y. Zhao, P. D. Fan, R. J. Harrison, M. Dupuis, D. M. A. Smith, J. Nieplocha, V. Tipparaju, M. Krishnan, Q. Wu, T. V. Voorhis, A. A. Auer, M. Nooijen, E. Brown, G. Cisneros, G. I. Fann, H. Fruchtl, J. Garza, K. Hirao, R. Kendall, J. A. Nichols, K. Tsemekhman, K. Wolinski, J. Anchell, D. Bernholdt, P. Borowski, T. Clark, D. Clerc, H. Dachsel, M. Deegan, K. Dyall, D. Elwood, E. Glendening, M. Gutowski, A. Hess, J. Jaffe, B. Johnson, J. Ju, R. Kobayashi, R. Kutteh, Z. Lin, R. Littlefield, X. Long, B. Meng, T. Nakajima, S. Niu, L. Pollack, M. Rosing, G. Sandrone, M. Stave, H. Taylor, J. L. G. Thomas, A. Wong, and Z. Zhang, Version 5.1 ed. (Pacific Northwest National Laboratory, Richland, Washington 99352, 2007).
[63] S. F. Boys and R. Bernardi, Mol. Phys. **19**, 553 (1970).
[64] F. B. van Duijneveldt, J. G. C. M. van Duijneveldt de Rijdt, and J. H. van Lenthe, Chem. Rev. **94**, 1873 (1994).
[65] C. Y. Peng and H. B. Schlegel, Isr. J. Chem. **33**, 449 (1994).
[66] See supplementary material at http://dx.doi.org/10.1063/1.3292646 for two figures comparing total cross sections from collision-induced dissociation of $Sr^{2+}(H_2O)_5$ and $Sr^{2+}(H_2O)_6$ complexes generated with the ESI and DC/FT sources and three tables providing geometrical parameters of $Sr^{2+}(H_2O)_x$ complexes.
[67] M. Beyer, E. R. Williams, and V. E. Bondybey, J. Am. Chem. Soc. **121**, 1565 (1999).
[68] A. A. Shvartsburg and K. W. M. Siu, J. Am. Chem. Soc. **123**, 10071 (2001).

Downloaded 02 Dec 2010 to 155.97.11.184. Redistribution subject to AIP license or copyright; see http://jcp.aip.org/about/rights_and_permissions